

# ACS Distortion derived from RAS-HOMS Measurements

---

Colin Cox and Don Lindler.  
January 28, 2002

---

## ABSTRACT

*In the February 2001 calibration campaign at Ball Aerospace, measurements were made using RAS-HOMS. Two sets of measurements were performed to derive the ACS distortion patterns. A Ronchi ruling was placed at the image plane to provide a reference square grid. Also a series of laser point images were placed at measured positions to simulate stellar images. The ruling measurements define the shape of the distortion while the laser images give the absolute location in the vehicle frame. Analysis of the two sets of data provides the complete solution for the ACS detectors. We describe how the various aperture positions are defined and their properties calculated. Results of the analysis are supplied to the Science Instrument Aperture File and the ACS Image Distortion Coefficients calibration table.*

---

## Introduction

The ACS exhibits considerable distortion. The scale is non-isotropic and over the field of view of the WFC varies by about 10%. A good understanding of this distortion is essential both for accurate pointing, especially for coronagraphic observations and for analysis of images where details of shape and relative positions are of interest. A weak gravitational lensing study will be an important part of the ACS program. This involves measuring distortions of galaxy images produced by gravitational lenses. It will be important to be able to discriminate between this effect and the distortion produced by the telescope optics.

## Measurements

Measurements were made in the Reflected Aberrated Simulator (RAS) at Ball Aerospace. A Ronchi ruled grating was placed at the object plane and the ACS detectors aligned to be at the focus. Images were taken with the WFC and HRC cameras. Illumination was with a HeNe laser corresponding to the 633 nm design wavelength of the RAS. (An attempt to illuminate using a tungsten lamp produced images that were difficult to interpret due to chromatic aberration.) Figure 1 is an image measured by a single WFC chip and Figure 2 shows

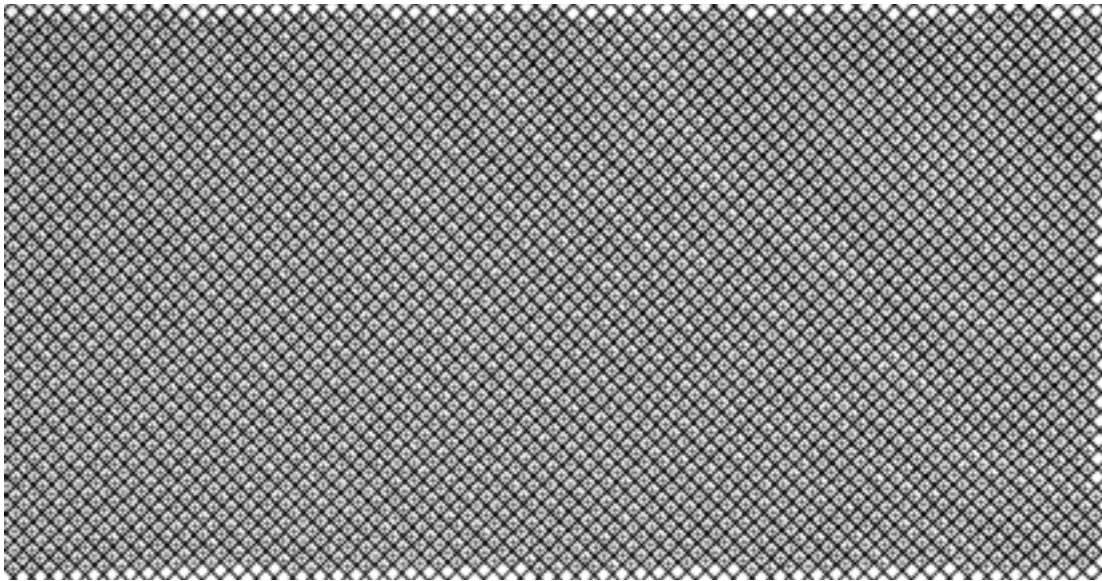


**Figure 1:** Ronchi ruling image for a single WFC chip. The plus signs within each diamond shape are not part of the original image, but indicate successful identification of each diamond pattern element by the cross-correlation software

an HRC image of the grating. The position of the center of each diamond shape is first determined approximately by a program which uses a cross-correlation with a single diamond image. A second pass profiles each of the diamond sub-sections and makes a more accurate determination of the center position. A two-dimensional polynomial fit is made of grid position versus pixel position. No knowledge of the size of the grid is needed, only that the positions are uniformly spaced. Measurements were taken with the grid rotated by  $90^\circ$  in case there was any difference in grid step size between the two axes. No difference was detected. The form of the distortion and the relative scales as a function of position and orientation are determined by this part of the analysis.

To obtain the absolute scales, orientations, and position of the detectors in telescope coordinates a second set of measurements was made. The grid is replaced by a plate with accurately positioned holes connected by fiber-optic cables to a laser output. The position of these simulated stars was previously determined by measurements made on the RAS. By measuring the centroids of the laser spot images on the detectors we can relate the pixel positions to vehicle ( $V_2, V_3$ ) coordinates. (For the HRC, the extent of the image is small compared to the diameter of the fiber-optic cable, so in reality a single point is used and moved around using a micrometer.)

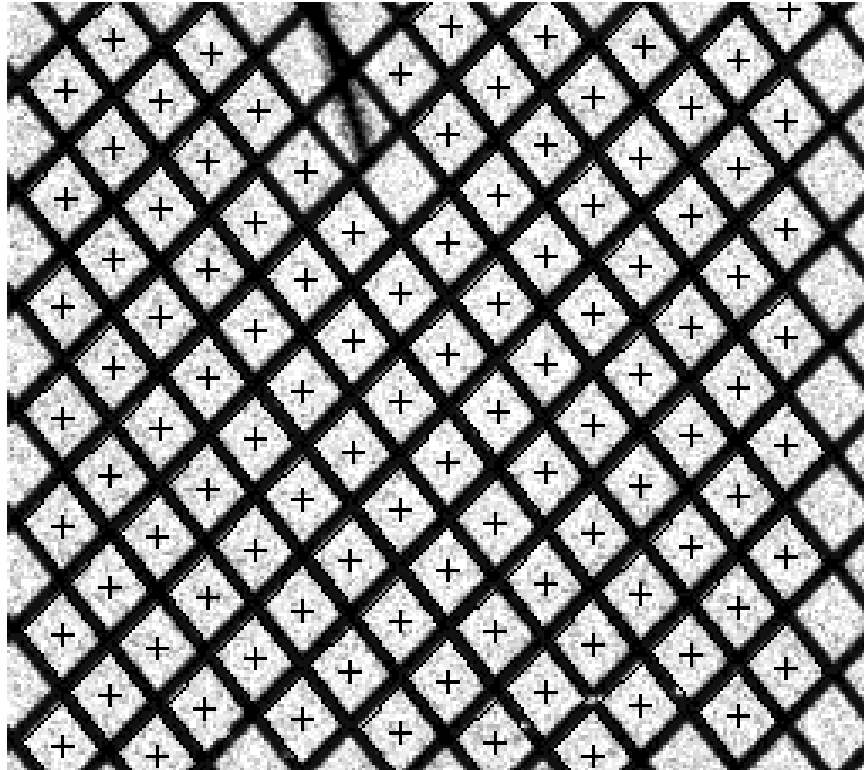


**Figure 2:** Ronchi ruling on HRC image. The coronagraphic finger is visible at the upper edge. Diamonds shadowed by the finger are not correctly located by the software and are omitted from the analysis.

### Analysis

From the first set of measurements we obtain a set of pixel positions  $(x, y)$  and a matching set of grid positions  $(x_g, y_g)$ . The grid positions are integer and somewhat arbitrary since the origin depends on which diamond is chosen as the starting point. However, by inspection it is not difficult to align different grid images since each grid step corresponds to about 45 WFC pixels or 90 HRC pixels.

The second set of measurements relates distorted  $(x,y)$  positions to an undistorted  $(V2,V3)$  frame. The distortion is the same for the grid measurements as for the  $V2V3$  measurements and the  $(x_g,y_g)$  are linearly related to  $(V2,V3)$ , both being independent of the optics. By combining the two sets of measurements we can extract both the distortion and the absolute location of the image.

The first complication to be dealt with is the various sets of coordinates used by different parts of the operation.

**Coordinate systems**

The IDL software used by the science team is in terms of what we will call display coordinates  $(X,Y)$  which in Figure 3 are in the normal orientation with the bottom left pixel being numbered  $(0,0)$ . The  $(Axis1,Axis2)$  user coordinates, i.e the coordinates which will be used for display of raw images in iraf, are inverted in the y-direction. Furthermore they start at  $(1,1)$  and include the physical overscan pixels. For the WFC chips there are 24 at the left and right edges as illustrated, making the detector area 4144 by 2048. So  $(0,0)$  in the  $(X,Y)$  system is  $(25,2048)$  in the  $(Axis1,Axis2)$  system. The relationship between them is

$$Axis1=X+25, Axis2=2048-y$$

For the purposes of developing the distortion fit, a coordinate set  $(x,y)$ , based on the user coordinates but with origin at a central point  $(2072,1024)$  is used.

The relationship between these coordinates and  $(X,Y)$  is

$$x=Axis1-2072= X-2047$$

$$y=Axis2-1024 =1024-Y$$

For the HRC, the overscan is 19 pixels at each edge and the user coordinates refer to a 1062 by 1024 area with a central reference point at  $(531,512)$ . The  $(0,0)$  corner occurs at the corner nearest the readout amplifier used. When amplifier C is used, as was the case during the February calibrations,  $x$  increases with  $X$  and  $y$  is still inverted with respect to  $Y$ . The relationships are

$$Axis1 = X + 20, Axis2 = 1024-Y$$

and

$$x = X-511, y = 512-Y$$

Since  $x$  and  $y$  are defined by the center of the detector, the relationship between  $(x,y)$  and  $(X,Y)$  is unaffected by the overscan numbers.

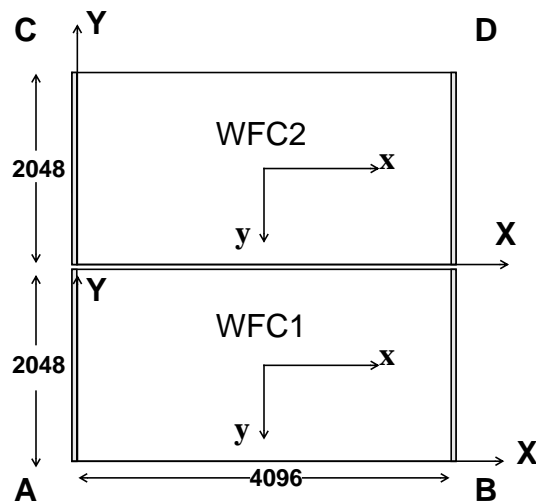


**Figure 3:** Instrument team coordinate system  $(X,Y)$  and shifted user coordinate system  $(x,y)$  for WFC

**Connecting to telescope coordinates**

The first phase of the analysis takes the grid points  $x_g, y_g$  and fits them as a function of the pixel centers located by the program *diamondfind*. The program was given this name because the grid is imaged at about 45 degrees and the squares appear as diamonds. The solution is expressed in the form

$$x_g = \sum_{i=0}^k \sum_{j=0}^i A_{i,j} \cdot x^j \cdot y^{i-j} \quad y_g = \sum_{i=0}^k \sum_{j=0}^i B_{i,j} \cdot x^j \cdot y^{i-j}$$

From the measurements using the simulated stars we obtain a set of  $(x,y)$  pixel values matching a set of  $(V2, V3)$ . We assume that the  $(V2, V3)$  positions are linearly related to the grid positions, and it only remains to determine the absolute location, scales and orientations which are expressed by a 6-parameter fit. To do this, we take each  $(x,y)$  position, calculate a set of  $(x_g, y_g)$  positions using the A and B coefficients, thereby taking out the distortion. Then we do a linear fit against the matching  $(V2, V3)$  values. We may express the results as

$$\begin{bmatrix} V2 - V2_0 \\ V3 - V3_0 \end{bmatrix} = \begin{bmatrix} L_{11} & L_{12} \\ L_{21} & L_{22} \end{bmatrix} \cdot \begin{bmatrix} x_g \\ y_g \end{bmatrix} = \begin{bmatrix} L_{11} & L_{12} \\ L_{21} & L_{22} \end{bmatrix} \cdot \begin{bmatrix} A(x, y) \\ B(x, y) \end{bmatrix} = \begin{bmatrix} a(x, y) \\ b(x, y) \end{bmatrix}$$

$A(x,y)$  and  $B(x,y)$  are functions of  $x$  and  $y$  represented by the polynomial expansion given above. The linear operator,  $L$ , a 2 by 2 matrix, is applied to the  $A$  and  $B$  coefficients to give the  $a$  and  $b$  set, which convert directly from  $(x,y)$  to  $(V2, V3)$ .

The point  $(V2_0, V3_0)$  corresponds to the reference point where  $x$  and  $y$  are zero. To obtain solutions which apply to a reference point displaced by  $(x_a, y_a)$  from the original point, as will be required for special apertures, a new set of coefficients  $a', b'$  may be obtained according to:

$$a'_{p,q} = \sum_{i=p}^k \sum_{j=q}^{i-(p-q)} {}^j C_q^{i-j} C_{p-q}^{i-j} x^j y^{i-j} a_{i,j}$$

with a similar form for  $b'$ . In this formula,  ${}^j C_q$  represents the combinatorial function giving the number of ways of selecting  $q$  items from a set of  $j$  items. The derivation of this formula is given in the appendix.

These displaced solutions are only necessary to accommodate the conventions and format of the Science Instrument Aperture File, (SIAF). The contents of the SIAF for the ACS as related to the distortion coefficients are described in TIR ACS 99-002 (Cox 1999). Normally, to perform a position calculation one would use the  $x$  and  $y$  offsets from the original reference point and the basic solution, avoiding the complications of calculating a new set of coefficients. The two methods are mathematically equivalent. This and other complications arise only because, for the first time, non-linear terms are included in the SIAF. Previous HST instruments have exhibited a small amount of distortion which has

been calibrated and compensated for in analysis. The ACS distortion is sufficient to impact telescope pointing and must be allowed for in planning observations and therefore included in the SIAF.

We now have a set of coefficients which convert from pixel position to  $(V2, V3)$ . This solution is used both for the SIAF and to generate dither coefficients, but in neither case are these coefficients used exactly as presented so far. For the dither and mosaicing application, the final coordinate system is aligned with the  $(V2, V3)$  but with the same parity as the original  $(x, y)$  coordinates. For the WFC this means that the dither x-axis is parallel to  $V2$  but the y-axis is anti-parallel to  $V3$ . Furthermore, the axes are scaled and shifted to make a new set of virtual pixels that encompass the real pixels. Details are given in Instrument Science Report ACS 2001-008(Hack and Cox, 2001).

The SIAF interposes another coordinate system called the Science Instrument Corrected System (SICS) which is similar to the  $(V2, V3)$  system, being undistorted and measured in arcseconds. There is a separate one of these for each aperture with its origin at the aperture reference point and with its y-axis parallel to the y pixel direction at this point. The angle, measured from  $V3$  to the y-axis in an anti-clockwise direction looking along the  $V1$  axis, is labelled  $\theta$ . The SICS y-axis is at right angles to the SICS x-axis such that the rotation from SICS x to SICS y is in the same sense as from x to y. The  $(V2, V3)$  axes also form an orthogonal set, but for most HST instruments, including the ACS, are in the opposite sense. We express this by a parity factor  $p$  set to -1.

The relationship between these coordinates may be given in one direction by

$$\begin{aligned} V2 - V2_0 &= px_c \cdot \cos\theta + y_c \cdot \sin\theta \\ V3 - V3_0 &= -px_c \cdot \sin\theta + y_c \cdot \cos\theta \end{aligned}$$

and in the other direction by

$$\begin{aligned} x_c &= p(V2 - V2_0) \cdot \cos\theta - p(V3 - V3_0) \cdot \sin\theta \\ y_c &= (V2 - V2_0) \cdot \sin\theta + (V3 - V3_0) \cdot \cos\theta \end{aligned}$$

The set of coefficients  $a'', b''$ , which convert from pixels  $(x, y)$  to the SICS coordinates,  $x_c, y_c$  are obtained from the  $a', b'$  set by applying this last transformation.

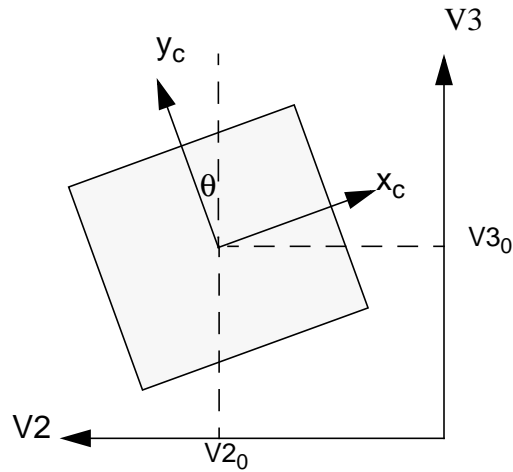


**Figure 4:** The Science Instrument Corrected System  $(x_c, y_c)$  and its relationship to  $(V2, V3)$ . The  $V1$  axis goes into the page.

$$a''_{i,j} = pa'_{i,j} \cdot \cos\theta - pb'_{i,j} \cdot \sin\theta$$

$$b''_{i,j} = a'_{i,j} \cdot \sin\theta + b'_{i,j} \cdot \cos\theta$$

Because of the way  $\theta$  is defined,  $a''_{10}$  is always equal to 0. This is equivalent to saying that the  $y$  and  $y_c$  axes are parallel. This final set of coefficients is installed in the SIAF together with the angle  $\theta$ .

### **Compact Notation**

We also have a need for the inverse solution which converts undistorted positions measured in arcseconds back to pixel locations. To simplify the typing and possibly to make the argument easier to follow, we define the following vectors representing the pixel values, the grid positions, the telescope coordinates and the SICS system respectively.

$$X = \begin{bmatrix} x \\ y \end{bmatrix} \quad G = \begin{bmatrix} x_g \\ y_g \end{bmatrix} \quad V = \begin{bmatrix} V2 - V2_0 \\ V3 - V3_0 \end{bmatrix} \quad S = \begin{bmatrix} x_c \\ y_c \end{bmatrix}$$

The previously stated equations may be restated more succinctly as  $G=A(X)$ , meaning that the vector  $G$  is a function of  $X$ , expressed by the coefficients  $a$  and  $b$ .

$$V=L.G \text{ indicates multiplying } G \text{ by the matrix, } L = \begin{bmatrix} L_{1,1} & L_{1,2} \\ L_{2,1} & L_{2,2} \end{bmatrix}$$

The set of coefficients  $a', b'$  represented by  $A'$  are defined by  $V=A'(X)$ . Also  $V=L.G=L.A(X)$ , so that  $A'=L.A$  as stated at greater length above.

We further define the linear transformation from  $S$  to  $V$  by a second matrix  $R$  involving just a rotation and a parity inversion, so that  $V=R.S$ . The final coefficients  $A''$ , giving  $S$  in terms of  $X$  are formally represented by  $S=A''(X)$ . We may write  $S = R^{-1}V = R^{-1}A'(X)$ . So finally,  $A''=R^{-1}A' = R^{-1}LA$  as derived above.

$$\text{In these last steps } R = \begin{bmatrix} p \cos\theta & \sin\theta \\ -p \sin\theta & \cos\theta \end{bmatrix} \quad R^{-1} = \begin{bmatrix} p \cos\theta & -p \sin\theta \\ \sin\theta & \cos\theta \end{bmatrix}$$

(Since  $p = -1$  it turns out the two transformations are identical.)

Inverting the linear transformations is a simple matter but inverting the functions, as is required to derive the inverse solution, is more involved.

### **The inverse solutions**

As before we begin with a fit relating  $(x_g, y_g)$  to the diamond centers measured in  $(x, y)$  but in this case we express the  $(x, y)$  values as functions of  $(x_g, y_g)$ .

$$x = \sum_{i=0}^k \sum_{j=0}^i c_{i,j} \cdot x_g^j \cdot y_g^{i-j} \quad y = \sum_{i=0}^k \sum_{j=0}^i d_{i,j} \cdot x_g^j \cdot y_g^{i-j}$$

This inverse solution is not obtained from the forward solution, but rather it is an independent fit with the variables used in the reverse order. The two solutions are not precise inverses of each other, but each is equally valid and represents the measured data within experimental error. In the compact notation the inverse description is  $X=C(G)$ . We wish to find first a solution of the form  $X=C'(V)$ . i.e a set of coefficients which transform from (V2,V3) to pixels.

The linear relations given in the previous section are still applicable and are easily inverted. We may write  $G=L^{-1}V$  and hence  $X = C(G) = C(L^{-1} \cdot V)$ . The relationship  $G = L^{-1}V$  may be written explicitly as  $x_g = \alpha V2 + \beta V3$  and  $y_g = \gamma V2 + \delta V3$ . The first expression becomes

$$x = \sum_{i=0}^k \sum_{j=0}^i c_{i,j} \cdot (\alpha V2 + \beta V3)^j \cdot (\gamma V2 + \delta V3)^{i-j}$$

which we wish to express as

$$x = \sum_{p=0}^k \sum_{q=0}^p c'_{p,q} \cdot V2^q \cdot V3^{p-q}$$

By performing the binomial expansion of the expressions in parentheses and collecting terms involving  $V2^q V3^{p-q}$  we get

$$c'_{p,q} = \sum_{\mu=0}^q \sum_{j=\mu}^{\mu+(p-q)} {}^j C_{\mu} \cdot {}^{p-j} C_{q-\mu} \cdot \alpha^{\mu} \beta^{j-\mu} \gamma^{q-\mu} \delta^{(p-q)-(\mu-j)} \cdot c_{i,k}$$

with a parallel formula for  $d'_{i,j}$ . Extending this method, we also need the coefficients which transform from SICS coordinates to pixels. Expressing this as  $X = C''(S) = C''(R^{-1}V)$  we see that the same formulae apply in obtaining the  $c_{ij}$  coefficients from  $c_{ij}'$  but with  $\alpha, \beta, \gamma, \delta$  being the elements of  $R^{-1}$ . Details of the coefficient calculations are given in the appendix.

## Special Apertures

### *Polarizers*

The distortion solutions for most of the ACS apertures may be obtained from those generated for the main solution for each detector by shifting to each reference point as described above. For the polarizer apertures and the HRC coronagraph, separate solutions are required. Measurements made in February 2001 revealed slight changes of scale with use of the polarizers. The displacements were measured by imaging the Ronchi ruling with

and without the polarizers and performing fits as before. A summary of the displacements and scale changes is given in Table 1. The V2 and V3 shifts represent the change in the reference point and the changes of scale are compared to the unpolarized case. For the UV polarizers, there was no unpolarized measurement made with a matching grid placement, so we currently assume zero average displacement and give relative displacements. We will rely on in-flight measurements for these apertures. Even for the visible polarizers, on-sky measurements will be needed and will supersede the ground values.

	V2 shift (arcsec)	V3 shift (arcsec)	Scale change (%)
WFC1 POL0V	0.16	-0.19	0.8
WFC1 POL60V	0.05	-0.23	0.7
WFC1 POL120V	0.03	-0.30	0.8
WFC2 POL0V	0.01	-0.02	.08
WFC2 POL60V	-0.08	-0.08	0.7
WFC2 POL120V	-0.10	-0.16	0.8
WFC1POL0UV	0.06	0.07	0.6
WFC1POL60UV	-0.02	-0.01	0.6
WFC1POL120UV	-.04	-.06	0.6
WFC2POL0UV	0.05	0.08	0.6
WFC2POL60UV	-0.02	-0.01	0.6
WFC2POL120UV	-0.03	-0.07	0.6
HRCPOL0V	-0.12	0.07	-1.5
HRCPOL60V	-0.05	0.15	-1.6
HRCPOL120V	-0.06	0.22	-1.5
HRCPOL0UV	-0.03	-0.07	-0.3
HRCPOL60UV	0.02	-0.02	-0.3
HRCPOL120UV	0.01	0.05	-0.3

**Table 1.** Polarizer induced shifts and scale changes

### *The HRC Coronagraph*

The coronagraph plate causes a displacement of about 0.2 arcseconds but no measurable scale change. The procedure for placing a target behind the coronagraphic spot will be to first locate it with the coronagraph out of the light path. When the coronagraph is inserted we require that the target image moves behind the 1.8 arcsecond spot. The 1.8 arcsecond coronagraphic spot appears at position (533,467). Inserting the coronagraphic plate causes a star to be shifted by (-7,+8) pixels. Targets will be acquired at position (540, 459) so that deploying the coronagraph moves the target under the occulting spot. The 3.0 arcsecond

coronagraphic spot appears at (438,795). The position chosen under the occulting finger is at (435,796). Again, note that all of this is based on illumination by an OTA simulator and the true positions will be measured in-flight during the SMOV to correct and refine these values.

### Micro-channel plate distortion

The construction of the micro-channel plate causes a small amount of distortion independent of the optical effects. Small irregularities in the placement of individual fibers show up as shifts in the positions of image pixels

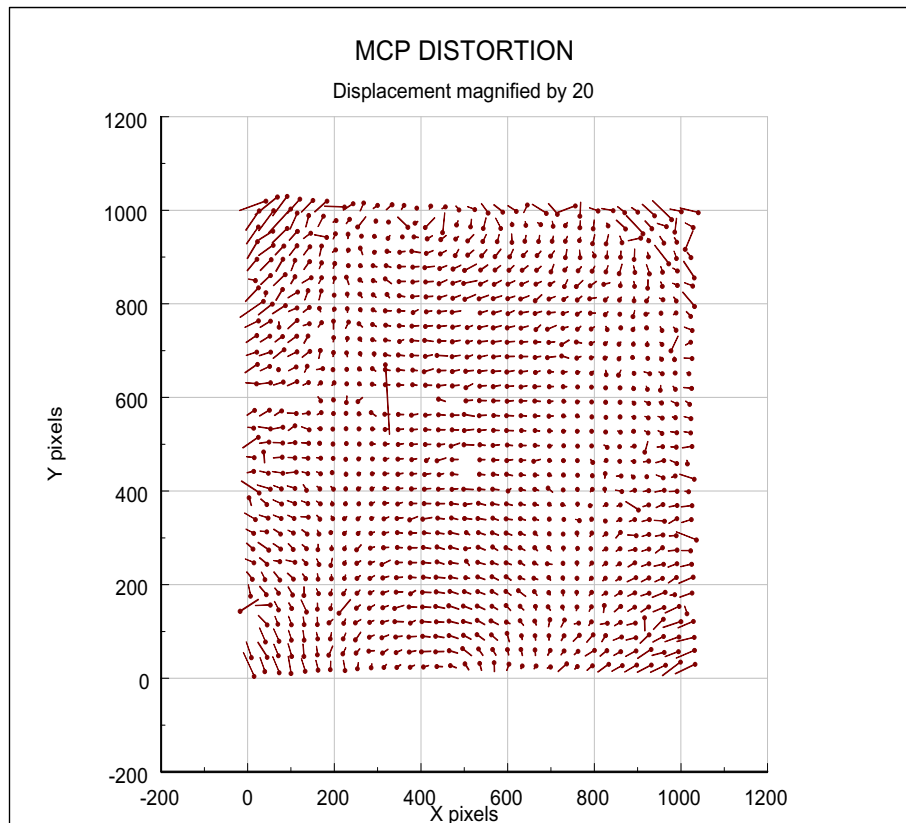


**Figure 5:** Intrinsic distortion of the micro-channel plate

A grid pattern was placed in contact with the face plate of the MAMA and illuminated with a diffuse source. In this way, the image produced is not affected by any external optics. The resulting image was analyzed by finding the centroid of each projected grid position and then fitting these positions to a uniformly spaced pattern. The deviations from uniformity are shown in Figure 5. The mean deviation is around 0.8 pixels with some values being several pixels in magnitude. The pattern has been sub-sampled by a factor of 3 for the purposes of display. The empty area near row 600 is due to a broken anode. Although there are some localized swirl patterns, overall the distortion can be fit well by a

cubic polynomial in  $x$  and  $y$  with a residual RMS deviation of about 0.3 pixels. Therefore the SBC can be treated in the same way as the HRC when on-sky measurements are taken. The intrinsic MCP distortions will convolve with the optical distortion to give a solution slightly different from that for the HRC, but of the same form. It will not be necessary to explicitly allow for the MCP distortion.

## Results

The fitting results are essentially the same as were presented in TIR ACS 99-002 which was based entirely on Code V modelling. The current values are derived from an HST optical simulator feeding into the real ACS. The two WFC chips have been treated separately whereas before, an overall solution was used with a reasonable estimate of their relative positions. The inter-chip gap was taken as 30 pixels. The current results show that the true value is close to 50 pixels. The scales and the variation in scales remain as predicted. Although the values presented here are useful for planning and exercising the drizzle software they will be superseded by in-flight calibration and the SIAF will be updated following analysis of those measurements.

### *Wide Field Camera*

Solutions were obtained separately for each chip. Coefficients are presented in the following tables and represent transformations between pixels ( $x, y$ ) and vehicle coordinates, ( $V2, V3$ ). The root-mean-square error is 0.2 pixels

The results describe the absolute location of each chip and thereby the relationship between them. In particular, the inter-chip gap is demonstrated to be about 2.5 arcseconds, varying between 50 and 53 pixels in width, and WFC1 is displaced about 3.5 pixels in the negative  $x$  direction compared to WFC2.

The  $a_{0,0}$  and  $b_{0,0}$  coefficients are zero by definition. The  $c_{0,0}$  and  $d_{0,0}$  values might also be expected to be zero. They deviate by an insignificant few hundredths of a pixel because the inverse solution is not quite identical to the forward one, and the connection between the reference ( $V2, V3$ ) and reference pixel has been defined by the forward solution.

The major feature of the distortion is the variation in  $x$  and  $y$  scales shown in Figure 6 and Figure 7. Overall the variation is about 5%. Because of the distortion, lines of constant  $x$  or  $y$  are slightly curved in the ( $V2, V3$ ) frame of reference. The aperture position angle therefore has to be defined at a particular point which we will choose as the reference point. The aperture position angle is defined as the angle from the  $V3$  axis to the aperture  $y$  axis, measured anti-clockwise. the angle  $\theta$  can therefore be calculated as

$\tan \theta = \frac{\partial V2}{\partial y} / \frac{\partial V3}{\partial y}$  which at the reference point is  $a_{1,0} / b_{1,0}$  For WFC1 the angle is 177.6 degrees while for WFC2 it is 178.0 degrees. At the WFC reference point, (2072,200) on WFC1, the angle is 177.8 degrees.

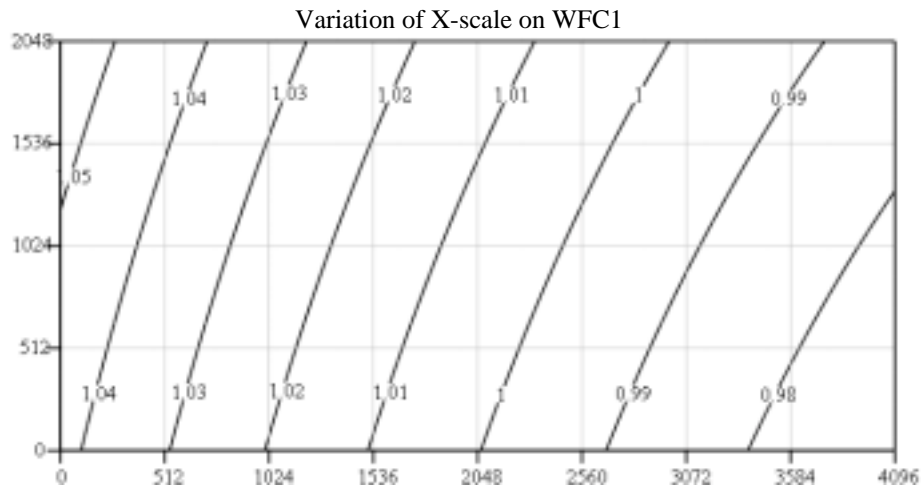
i,j	WFC1		WFC2	
	$a_{i,j}$	$b_{i,j}$	$a_{i,j}$	$b_{i,j}$
0,0	0	0	0	0
1,0	0.002032	-0.048949	0.001718	-0.050679
1,1	0.049160	-0.002231	0.049779	-0.001583
2,0	$1.029 \times 10^{-7}$	$4.904 \times 10^{-7}$	$9.929 \times 10^{-8}$	$3.677 \times 10^{-7}$
2,1	$-3.527 \times 10^{-7}$	$-2.955 \times 10^{-7}$	$-2.541 \times 10^{-7}$	$-3.068 \times 10^{-7}$
2,2	$4.240 \times 10^{-7}$	$1.304 \times 10^{-7}$	$4.316 \times 10^{-7}$	$8.124 \times 10^{-8}$
3,0	$4.461 \times 10^{-12}$	$1.571 \times 10^{-11}$	$-1.055 \times 10^{-13}$	$1.960 \times 10^{-11}$
3,1	$-2.258 \times 10^{-11}$	$1.996 \times 10^{-12}$	$-2.606 \times 10^{-11}$	$4.799 \times 10^{-12}$
3,2	$-5.327 \times 10^{-12}$	$1.846 \times 10^{-11}$	$-2.602 \times 10^{-12}$	$2.736 \times 10^{-11}$
3,3	$-2.187 \times 10^{-11}$	$-3.686 \times 10^{-12}$	$-2.286 \times 10^{-11}$	$-3.714 \times 10^{-12}$

**Table 2.** Forward solutions for the Wide Field Camera. The (V2,V3) reference positions for WFC1 and WFC2 are (258.02, 196.40) and (254.26, 301.11). The coefficients in the Image Distortion Correction file may be obtained from this table by changing the sign of the  $b_{i,j}$

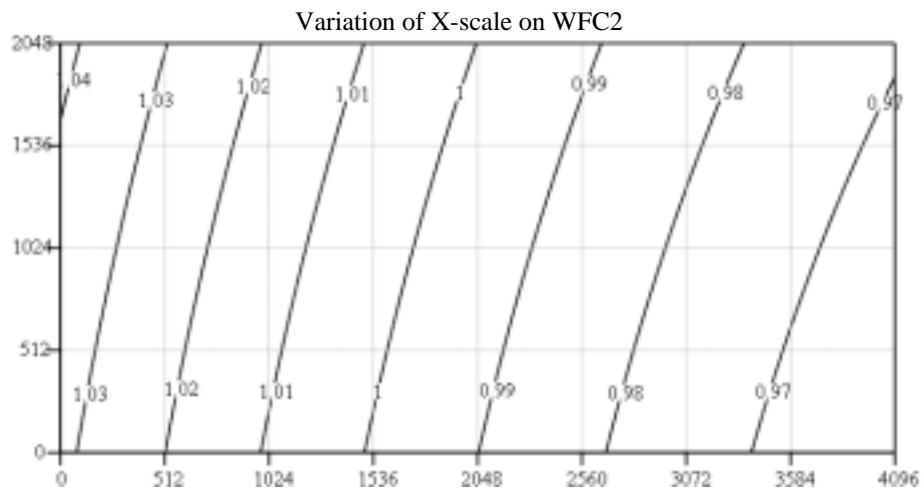
i,j	WFC1		WFC2	
	$c_{i,j}$	$d_{i,j}$	$c_{i,j}$	$d_{i,j}$
0,0	0.0485	-0.0284	0.0483	-0.0221
1,0	0.8463	-20.4683	0.6817	-19.7535
1,1	0.3801	-0.9288	20.1107	-0.6284
2,0	$-1.210 \times 10^{-3}$	$4.386 \times 10^{-3}$	$-9.711 \times 10^{-4}$	$2.963 \times 10^{-3}$
2,1	$-3.544 \times 10^{-3}$	$3.190 \times 10^{-3}$	$-2.438 \times 10^{-3}$	$2.737 \times 10^{-3}$
2,2	$-3.819 \times 10^{-3}$	$1.420 \times 10^{-3}$	$-3.640 \times 10^{-3}$	$8.540 \times 10^{-4}$
3,0	$1.661 \times 10^{-6}$	$-4.717 \times 10^{-6}$	$5.932 \times 10^{-7}$	$-3.965 \times 10^{-6}$
3,1	$6.068 \times 10^{-6}$	$-3.073 \times 10^{-6}$	$5.334 \times 10^{-6}$	$-1.535 \times 10^{-6}$
3,2	$2.593 \times 10^{-6}$	$-5.338 \times 10^{-6}$	$2.036 \times 10^{-6}$	$-5.640 \times 10^{-6}$
3,3	$5.391 \times 10^{-6}$	$-1.661 \times 10^{-6}$	$5.157 \times 10^{-6}$	$-1.255 \times 10^{-6}$

**Table 3.** Inverse solutions for the Wide Field Camera. To obtain the IDC table values,

multiply each entry by  $(-1)^{i+j}$ .

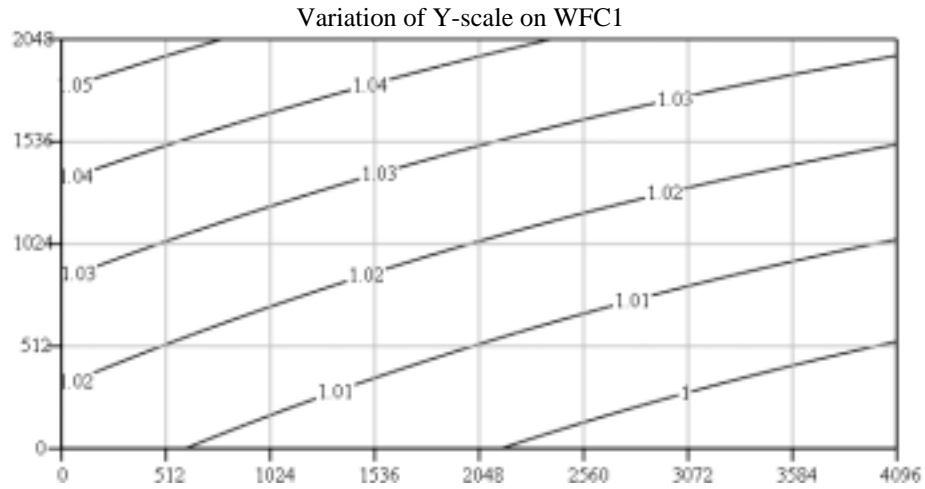


XS1

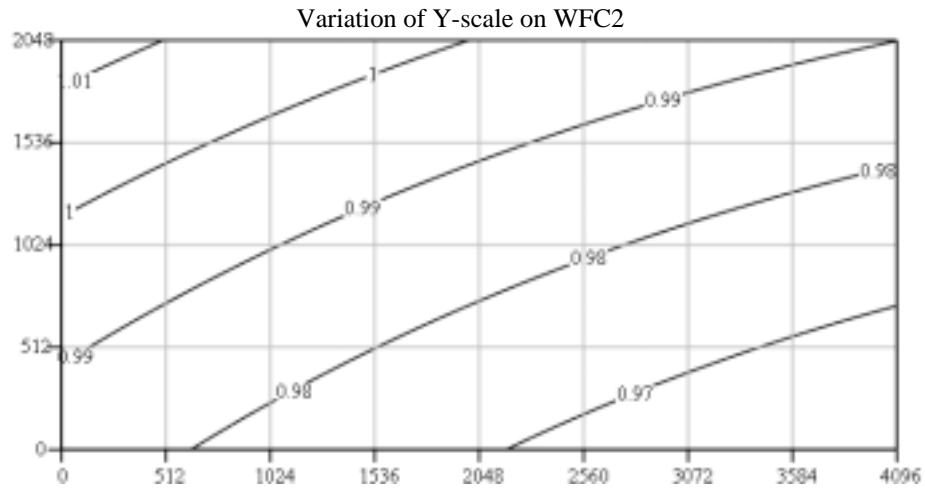


XS2

**Figure 6:** Variation of x-scale on the WFC detectors. Scales are normalized to the value midway between the chips which is 0.0497 arcsec/pixel



YS1



YS2

**Figure 7:** The variation of y-scale on the WFC detectors. Scales are normalized to a point mid-way between the detectors where the value is 0.0497 arc-sec/pixel

**High Resolution Camera**

The HRC, because it covers a much smaller area, shows much less variation in scale. The maximum variation from the central value is less than 0.5%. However there is considerable anisotropy; the scale in the x direction exceeds that in the y direction by 14%. The central x and y values are 0.02843 and 0.02485 arcsecond/pixel.

$i,j$	$a_{ij}$	$b_{ij}$	$c_{ij}$	$d_{ij}$
0,0	0	0	-0.0002	-0.0007
1,0	-0.000030	0.024694	-0.0424	40.5010
1,1	-0.028415	0.002804	-35.1967	3.9970
2,0	$3.998 \times 10^{-8}$	$2.771 \times 10^{-7}$	$2.347 \times 10^{-3}$	$-1.863 \times 10^{-2}$
2,1	$-2.373 \times 10^{-7}$	$-5.868 \times 10^{-8}$	$1.239 \times 10^{-2}$	$-8.422 \times 10^{-3}$
2,2	$1.047 \times 10^{-7}$	$3.675 \times 10^{-8}$	$5.774 \times 10^{-3}$	$-3.009 \times 10^{-3}$
3,0	$-9.507 \times 10^{-12}$	$6.095 \times 10^{-11}$	$-2.410 \times 10^{-5}$	$-1.448 \times 10^{-4}$
3,1	$2.084 \times 10^{-11}$	$-1.247 \times 10^{-11}$	$-6.023 \times 10^{-5}$	$-5.913 \times 10^{-5}$
3,2	$-6.676 \times 10^{-12}$	$3.535 \times 10^{-11}$	$-2.916 \times 10^{-5}$	$-7.264 \times 10^{-5}$
3,3	$2.627 \times 10^{-11}$	$2.432 \times 10^{-11}$	$-4.436 \times 10^{-5}$	$4.142 \times 10^{-5}$

**Table 4.** Forward and inverse solutions for the HRC. The (V2,V3) reference point is (205.14, 470.19) at the central pixel position (531,512), again including physical overscan pixels. The IDC table values reverse the sign of each  $a_{ij}$  and multiply each  $c_{i,j}$  by  $(-1)^j$ .

**Solar Blind Camera**

No distortion measurements were made for the SBC MAMA. The SBC lies at the end of the same optical path as the HRC except for the final M3 plane mirror. For the pre-flight values we will use the results from the HRC scaled by the pixel sizes which are  $21\mu$  for the HRC and  $25\mu$  for the SBC. No attempt has been made to incorporate the MAMA intrinsic distortion since we will measure the full distortion in orbit.

**Fine Guidance System Coordinates**

Up to this point calculations have been done in a V2,V3 coordinate system related to telescope and instrument metrology. Operationally, we measure sky positions with the interferometric Fine Guidance System (FGS). All positions are relative to these interferometers. Over the lifetime of HST they have moved by distances corresponding to several arcseconds and two of them have been replaced, so that now values in the FGS system, which we may label  $V2_f, V3_f$  are given by  $V2_f = V2 + 2.24$  and  $V3_f = V3 - 6.79$ , all values

in arcseconds. This has no effect on most of the calculations presented, but just implies an offset to all the aperture V2,V3 reference positions. The positions quoted with Tables 2 and 4 include these offsets. There is also a rotation of about 0.1 degrees. We choose to ignore this correction for the preflight data because the prediction of final location of the camera is probably uncertain by about this amount.

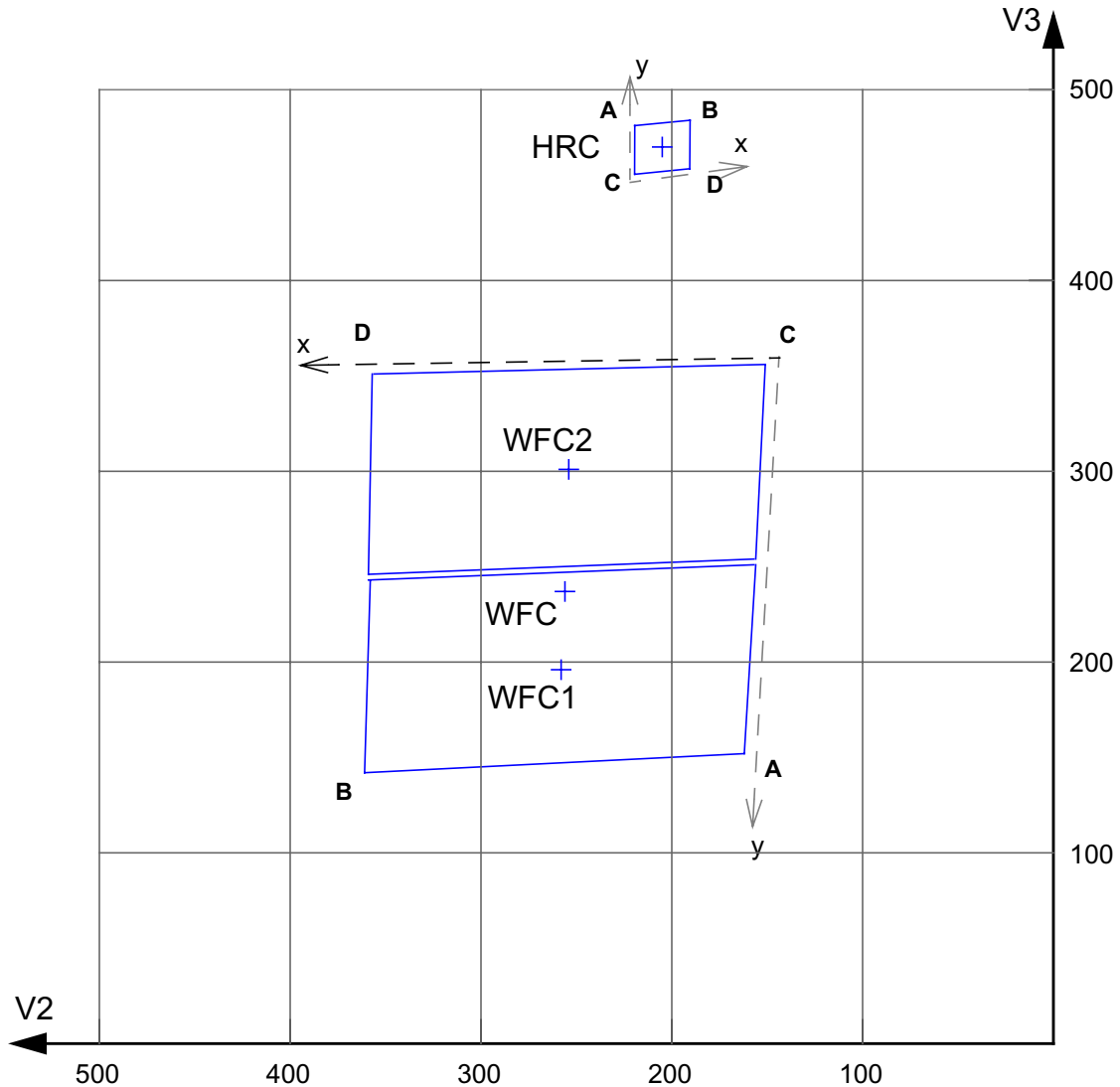


**Figure 8:** Positions of WFC and HRC in FGS ( $V_2, V_3$ ) coordinates. The directions of user coordinates are shown and the target reference points indicated. The pipeline will supply science images with the x-axis running from left to right and the y axis from bottom to top. The CCD amplifier corners are indicated to unambiguously define the orientation.

## **Acknowledgements**

Thanks are due to Bill Eichhorn of Goddard Space Flight Center and David Kubalak of Orbital Sciences Corporation for providing data and performing calculations with respect to the laser star measurements.

## **References**

Instrument Science Report ACS 2001-008, "Revised IDCTAB Definition: Application to HST Data", W Hack and C. Cox, July 2001.

Technical Instrument Report ACS 99-002 - Revision A, "The Science Instrument Aperture File for the ACS", C. Cox Dec. 1999

## Appendix: Details of coefficient transformations.

### *Shifting the distortion solution.*

The transformation from detector pixels  $(x,y)$  to  $(V2,V3)$  which arises directly from measurements will be expressed as order  $k$  polynomials

$$V2 = \sum_{i=0}^k \sum_{j=0}^i a_{i,j} x^j y^{i-j} \quad V3 = \sum_{i=0}^k \sum_{j=0}^i b_{i,j} x^j y^{i-j}$$

When a solution of the above form is given, the origin of the  $(x,y)$  system is often taken as the geometric center of the detector. Several apertures may be defined on the detector, each with their own  $(x,y)$  origin. Shifting the origin requires changes in the coefficients although the underlying relation between physical pixels and vehicle coordinates does not change. Suppose the new origin for coordinates  $(x',y')$  is at  $(xa, ya)$  so that  $x=x'+xa$ ,  $y=y'+ya$  and we are looking for a solution of the same form

$$V2 = \sum_{p=0}^k \sum_{q=0}^p a'_{p,q} x'^q y'^{p-q} \quad V3 = \sum_{p=0}^k \sum_{q=0}^p b'_{p,q} x'^q y'^{p-q}$$

Since the two forms describe the same relationship

$$\sum_{p=0}^k \sum_{q=0}^p a'_{p,q} x'^q y'^{p-q} = \sum_{i=0}^k \sum_{j=0}^i a_{i,j} (x'+xa)^j (y'+ya)^{i-j}$$

Performing the binomial expansion of the parentheses on the right hand side we get:

$$(x'+xa)^j = \sum_{\mu=0}^j {}^j C_{\mu} x'^{\mu} xa^{j-\mu} \quad (y'+ya)^{i-j} = \sum_{\nu=0}^{i-j} {}^{i-j} C_{\nu} y'^{\nu} ya^{i-j-\nu}$$

where  ${}^m C_n$  is the combinatorial function. Then the full expansion is

$$\sum_{p=0}^k \sum_{q=0}^p a'_{p,q} x'^q y'^{p-q} = \sum_{i=0}^k \sum_{j=0}^i \sum_{\mu=0}^j \sum_{\nu=0}^{i-j} a_{i,j} {}^j C_{\mu} {}^{i-j} C_{\nu} xa^{j-\mu} ya^{i-j-\nu} x'^{\mu} y'^{\nu}$$

Extracting from both sides the coefficient of  $x'^q y'^{p-q}$ , the left hand side gives  $a'_{pq}$ , the coefficients for the shifted solution. On the right hand side the terms which contribute to the coefficient for  $x'^q y'^{p-q}$  are those for which  $\mu=q$  and  $\nu=p-q$ . That is to say,  $\mu$  and  $\nu$  are fixed and the summations only run over  $i$  and  $j$ . From the form of the combinatorial functions  ${}^j C_{\mu}$  and  ${}^{i-j} C_{\nu}$ , we have the conditions that  $\mu \leq j$  and  $\nu \leq i-j$ . Substituting for  $\mu$  in the first condition gives  $q \leq j$  or equivalently  $j \geq q$ . Substituting for  $\nu$  in the second inequality gives  $p-q \leq i-j$ . Reordering gives  $i \geq p+(j-q)$  which, since  $j \geq q$ , means  $i \geq p$ . Using the same inequality in a different order gives  $j \leq i-(p-q)$ . So  $i$  runs from  $p$  to  $k$  and  $j$  from  $q$  to  $i-(p-q)$ .

$$a'_{p,q} = \sum_{i=p}^k \sum_{j=q}^{i-(p-q)} {}^j C_q {}^{i-j} C_{p-q} x^j y^{i-j} a_{i,j}$$

Although this looks cumbersome, it is easily implemented in a couple of program loops. A parallel equation holds for the  $b$  coefficients.

### ***The inverse solution***

The SIAF also requires sets of coefficients describing the transformation from SICS to detector coordinates. The same type of polynomial is used, namely

$$x = \sum_{i=0}^k \sum_{j=0}^i c_{i,j} \cdot x c^j \cdot y c^{i-j} \quad y = \sum_{i=0}^k \sum_{j=0}^i d_{i,j} \cdot x c^j \cdot y c^{i-j}$$

In our compact notation we expressed the inverse fit to the grid points as  $\mathbf{X}=\mathbf{C}(\mathbf{G})$  and we still have the relations  $\mathbf{V}=\mathbf{L}\cdot\mathbf{G}$  and  $\mathbf{V}=\mathbf{R}\cdot\mathbf{S}$  so that  $\mathbf{X}=\mathbf{C}(\mathbf{L}^{-1}\cdot\mathbf{V})$ . In this case, extracting coefficients that convert from  $(V2, V3)$  directly to  $(x,y)$  is more involved. We cannot simply apply  $\mathbf{L}^{-1}$  to the coefficients because it is involved in the polynomial expansion. The linear relationship  $\mathbf{G} = \mathbf{L}^{-1}\mathbf{V}$  may be written explicitly as  $x_g = \alpha V2 + \beta V3$  and  $y_g = \gamma V2 + \delta V3$ . The first expression becomes

$$x = \sum_{i=0}^k \sum_{j=0}^i c_{i,j} \cdot (\alpha V2 + \beta V3)^j \cdot (\gamma V2 + \delta V3)^{i-j}$$

which we wish to express as

$$x = \sum_{p=0}^k \sum_{q=0}^p c'_{p,q} \cdot V2^q \cdot V3^{p-q}$$

Performing the binomial expansion of the expressions in parentheses gives

$$x = \sum_{i=0}^k \sum_{j=0}^i \sum_{\mu=0}^j \sum_{\nu=0}^{i-j} {}^j C_{\mu} \cdot {}^{i-j} C_{\nu} \cdot \alpha^{\mu} \beta^{j-\mu} \gamma^{\nu} \delta^{i-j-\nu} \cdot c_{i,j} \cdot V2^{\mu+\nu} V3^{i-(\mu+\nu)}$$

As in the previous section, we extract the coefficient  $c'_{p,q}$  by picking out the  $c$  coefficients where  $\mu+\nu = q$  and  $i-(\mu+\nu) = p-q$ . This immediately gives  $\nu = q-\mu$  and  $i=p$ . The summation only runs over  $j$  and  $\mu$  with  $\nu = q-\mu$ . Since  $\nu$  must be positive,  $\mu \leq q$ . The combinatorial terms  ${}^j C_{\mu}$  and  ${}^{i-j} C_{\nu}$  lead to the limits  $0 \leq \mu \leq j$  and  $0 \leq q-\mu \leq p-j$ . These inequalities may be rearranged to read  $\mu \leq j \leq \mu+(p-q)$ . So finally  $\mu$  runs from 0 to  $q$ ,  $j$  runs from  $\mu$  to  $\mu+(p-q)$  and the  $c'$  coefficients are given by

$$c'_{p,q} = \sum_{\mu=0}^q \sum_{j=\mu}^{\mu+(p-q)} {}^j C_{\mu} \cdot {}^{p-j} C_{q-\mu} \cdot \alpha^{\mu} \beta^{j-\mu} \gamma^{q-\mu} \delta^{(p-q)-(\mu-j)} \cdot c_{p,j}$$

The final step is to obtain the  $c''$  and  $d''$  coefficients that connect  $(x,y)$  to the SICS coordinates. This requires one more coefficient calculation of the same form as this. Again we have to use a linear transformation  $R^{-1}$  for which the values of  $\alpha, \beta, \gamma, \delta$  above are respectively  $-\cos(\theta), \sin(\theta), \sin(\theta), \cos(\theta)$ . The preceding formula becomes

$$c''_{p,q} = \sum_{\mu=0}^q \sum_{j=\mu}^{\mu+(p-q)} j C_{\mu}^{p-j} C_{q-\mu}^{j-2\mu} \cdot (-1)^{\mu} \cos^{\mu} \theta \sin^{\mu} \theta \cdot c'_{p,j}$$